Journal of Ovonic Research Vol. 21, No. 2, March - April 2025, p. 163 - 176

Enhancement of friction behavior and self-healing capabilities in nitrile rubber through ZnO nanoparticles incorporation

X. G. Wang *, J. W. Qin, W. Li, L. Xie, X. M. Zheng
School of Petrochemical Engineering, Lanzhou Petrochemical University of Vocational Technology, Lanzhou 730060, Gansu, China

This study investigates a novel approach to enhance XNBR composites through the incorporation of synthesized ZnO nanoparticles with controlled morphology. The ZnO nanoparticles, synthesized via a modified co-precipitation method, exhibited uniform size distribution with 90% of particles ranging between 35-55 nm. Dynamic mechanical analysis revealed dual transition behavior, with a distinct ionic transition peak emerging above the glass transition temperature. The storage modulus at room temperature increased from 3.2 MPa to 7.8 MPa with 7.5 phr ZnO loading, while maintaining elongation at break above 600%. Tribological testing demonstrated significant improvements, with the composite achieving a 78% reduction in wear rate and maintaining stable friction coefficients under dry sliding conditions. Temperature-dependent self-healing studies showed progressive improvement in recovery rates, with maximum efficiency achieved at 80°C. The formation of ionic clusters, confirmed through FTIR analysis, played a crucial role in both mechanical reinforcement and self-healing mechanisms. The optimized composite demonstrated a 30% increase in crosslink density compared to conventional ZnO-cured systems, leading to enhanced thermal stability with char yield improving from 8% to 15% at 600°C.

(Received December 14, 2024; Accepted March 10, 2025)

Keywords: Ionic crosslinking, Mechanical reinforcement, Tribological enhancement, Thermal stability, Polymer nanocomposites

1. Introduction

Nitrile rubber (NBR) and its carboxylated variant (XNBR) represent crucial elastomeric materials in modern industrial applications, particularly in sectors demanding superior oil resistance and mechanical durability [1,2]. These materials find extensive use in automotive components, sealing systems, and protective equipment where sustained performance under demanding conditions is essential [3]. Despite their inherent advantages, these elastomers face persistent challenges regarding their tribological properties and long-term durability, especially in applications involving repeated mechanical stress and wear. The enhancement of rubber materials' performance characteristics, particularly their friction behavior and self-healing capabilities, has become increasingly critical in addressing industrial demands for extended service life and reduced

* Corresponding author: xinggangwang2024@163.com
https://doi.org/10.15251/JOR.2025.212.163

maintenance requirements [4]. Traditional approaches to improving rubber properties have primarily relied on conventional reinforcing agents and vulcanization systems [5]. However, these methods often result in compromised material properties, such as decreased elasticity or reduced processing efficiency, highlighting the need for innovative solutions that can simultaneously enhance multiple performance aspects.

The emergence of nanotechnology has opened new avenues for material enhancement, with zinc oxide (ZnO) nanoparticles emerging as particularly promising reinforcing agents for rubber matrices. Unlike conventional micro-sized ZnO particles traditionally used as curing agents, nanoscale ZnO particles offer unique advantages due to their high surface area-to-volume ratio and enhanced reactivity [6–8]. These characteristics potentially enable more efficient crosslinking and improved interface interactions with the rubber matrix, leading to superior mechanical and tribological properties. The incorporation of ZnO nanoparticles into nitrile rubber systems represents a sophisticated approach to addressing multiple material challenges simultaneously [9]. These nanoparticles can potentially serve dual functions: as effective curing agents and as nano-reinforcements [10]. Their nanoscale dimensions facilitate better dispersion within the rubber matrix, potentially leading to more uniform property enhancement throughout the material. Additionally, the high surface activity of ZnO nanoparticles suggests the possibility of forming more effective ionic crosslinks with carboxylated nitrile rubber, potentially enabling enhanced self-healing capabilities through reversible ionic interactions [1].

Self-healing capabilities in rubber materials represent a particularly significant advancement, as they offer the potential for extended material lifespans and reduced maintenance requirements [11,12]. The mechanism of self-healing in ZnO-modified rubber systems is hypothesized to operate through the formation and reformation of ionic bonds, enabling the material to recover from damage through molecular reconstruction at the damaged interfaces [13,14]. This capability could be particularly valuable in applications where regular maintenance or replacement is challenging or costly. The tribological behavior of rubber materials, including friction and wear characteristics, plays a crucial role in determining their practical applicability in various industrial settings. Traditional rubber compounds often struggle to maintain optimal friction coefficients while simultaneously resisting wear, particularly under aggressive operating conditions [15,16]. The introduction of ZnO nanoparticles offers potential solutions to these challenges through multiple mechanisms, including enhanced crosslinking density, improved interface strength, and modified surface properties [17]. Understanding the complex relationships between ZnO nanoparticle characteristics, processing conditions, and resulting material properties requires systematic investigation. The size, morphology, and distribution of ZnO nanoparticles within the rubber matrix can significantly influence the final material properties [18]. Moreover, the interaction between these nanoparticles and the rubber matrix at the molecular level plays a crucial role in determining both mechanical properties and self-healing capabilities.

The present study aims to investigate the comprehensive effects of ZnO nanoparticle incorporation on the enhancement of friction behavior and self-healing capabilities in nitrile rubber systems. Specifically, this research focuses on understanding the relationships between nanoparticle characteristics, processing conditions, and resulting material properties. Through detailed analysis of mechanical, tribological, and self-healing properties, this study seeks to establish clear structure-property-performance relationships that can guide future material development. The investigation encompasses multiple aspects of material behavior, including mechanical properties, tribological

characteristics, and self-healing efficiency. By examining these properties through various analytical techniques and testing methodologies, this research aims to provide a comprehensive understanding of the enhancement mechanisms involved. This knowledge is essential for optimizing material formulations and processing conditions to achieve desired performance characteristics for specific applications.

2. Materials and methods

2.1. Materials

XNBR with 27 wt% acrylonitrile content and 7.0 wt% carboxyl groups was supplied by Liaoning Synthetic Rubber Co., Ltd (Liaoning, China). The Mooney viscosity (ML 1+4 at 100°C) was 45±3, with a specific gravity of 0.98 g/cm³. Zinc nitrate hexahydrate ($Zn(NO_3)_2 \cdot 6H_2O$, 99.9% purity) and ammonium carbonate ($(NH_4)_2CO_3$, analytical grade) were obtained from Shanghai Macklin Biochemical Co., Ltd (Shanghai, China). Stearic acid and sulfur were procured from Tianjin Guangfu Technology Development Co., Ltd (Tianjin, China). Other chemical reagents including potassium hydroxide (KOH), zinc diethyldithiocarbamate (ZDEC), and dicumyl peroxide (DCP) were purchased from Sinopharm Chemical Reagent Co., Ltd (Shanghai, China). All chemicals were used as received without further purification.

2.2. Synthesis of ZnO nanoparticles

ZnO nanoparticles were synthesized using a modified co-precipitation method. Briefly, 1.0 M solutions of $Zn(NO_3)_2 \cdot 6H_2O$ and $(NH_4)_2CO_3$ were prepared separately in deionized water. The zinc nitrate solution was added dropwise to the vigorously stirred ammonium carbonate solution at a controlled rate of 2 mL/min, maintaining a molar ratio of 1:2. The reaction temperature was maintained at 25±2°C throughout the precipitation process. The resulting white precipitate was aged for 2 hours under continuous stirring at 500 rpm. The precipitate was collected through centrifugation at 8000 rpm for 15 minutes, followed by washing with deionized water and ethanol alternatively for five cycles. The washed precipitate was dried at 100°C for 12 hours in a vacuum oven, followed by calcination at 280°C for 2 hours to obtain the final ZnO nanoparticles.

2.3. Preparation of XNBR/ZnO nanocomposites

The XNBR compounds were prepared using a two-roll mixing mill at room temperature. The mixing sequence involved initial mastication of XNBR for 5 minutes, followed by sequential addition of stearic acid, ZnO nanoparticles, and other curatives. The nanoparticle loading was varied at 2.5, 5.0, 7.5, and 10.0 parts per hundred rubber (phr). Total mixing time was maintained at 15 minutes with a friction ratio of 1:1.2. The compounds were then sheeted out at 2 mm thickness and stored at room temperature for 24 hours before vulcanization. Vulcanization was performed using a hydraulic press at 150°C and 15 MPa pressure. The optimum cure time (t90) was determined using a moving die rheometer. Test specimens were prepared according to relevant standard specifications for different characterization techniques.

3. Results and discussion

3.1. ZnO Nanoparticle characterization

The morphological characteristics of synthesized ZnO nanoparticles were examined through SEM. Figure 1A reveals that the ZnO nanoparticles exhibit a predominantly rod-like morphology with an average length of 450±50 nm and diameter of 40±10 nm. The particles demonstrate a tendency to form one-dimensional assemblies, likely due to the preferential growth along the c-axis during synthesis [19]. Particle size distribution analysis, performed through dynamic light scattering, indicates a relatively narrow size distribution with 90% of the particles falling within the range of 35-55 nm in diameter (Figure 1B). This uniformity in particle size is advantageous for achieving consistent dispersion within the rubber matrix [20].

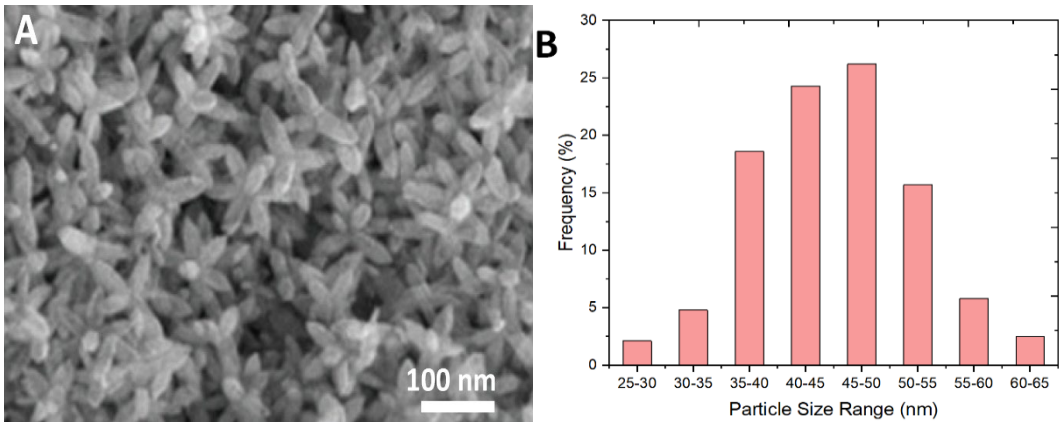

Fig. 1. (A) SEM micrograph of ZnO nanoparticles showing rod-like morphology; (B) Particle size distribution histogram of ZnO nanoparticles.

XRD patterns of the synthesized ZnO nanoparticles (Figure 2) exhibit characteristic peaks at 2θ values of 31.7°, 34.4°, 36.2°, 47.5°, and 56.6°, corresponding to the (100), (002), (101), (102), and (110) planes respectively [21]. These peaks match well with the hexagonal wurtzite structure of ZnO (JCPDS card no. 36-1451).

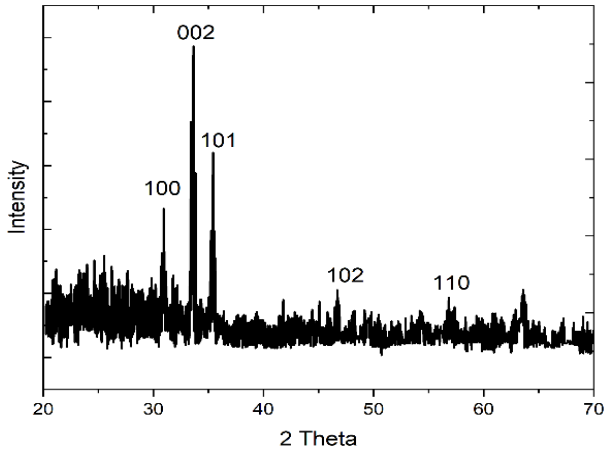

Fig. 2. XRD pattern of synthesized ZnO nanoparticles showing characteristic peaks of wurtzite structure.

3.2. Mechanical properties

The incorporation of ZnO nanoparticles significantly influences the mechanical properties of XNBR composites. Table 1 summarizes the key mechanical parameters for various ZnO loadings. The tensile strength shows a marked improvement with increasing ZnO content up to 7.5 phr, beyond which a slight decline is observed. At optimal loading (7.5 phr), the tensile strength reaches 18.5 MPa, representing a 125% increase compared to the unfilled XNBR (8.2 MPa).

Table 1. Mechanical properties of XNBR/ZnO composites at various ZnO loadings.

Property	**Unfilled XNBR**	**2.5 phr ZnO**	**5.0 phr ZnO**	**7.5 phr ZnO**	**10.0 phr ZnO**
Tensile Strength (MPa)	8.2 ± 0.4	12.4 ± 0.5	15.8 ± 0.6	18.5 ± 0.7	17.3 ± 0.7
Elongation at Break (%)	750 ± 25	720 ± 30	685 ± 28	645 ± 25	620 ± 30
Modulus at 100% (MPa)	1.2 ± 0.1	1.8 ± 0.1	2.5 ± 0.2	3.2 ± 0.2	3.4 ± 0.2
Modulus at 300% (M300) (MPa)	2.3 ± 0.2	3.4 ± 0.2	4.6 ± 0.3	5.8 ± 0.3	6.0 ± 0.3
Young's Modulus (MPa)	3.2 ± 0.2	4.8 ± 0.3	6.5 ± 0.3	7.8 ± 0.4	8.1 ± 0.4
Hardness (Shore A)	55 ± 2	62 ± 2	68 ± 2	73 ± 2	75 ± 2

The stress-strain curves (Figure 3) demonstrate the reinforcing effect of ZnO nanoparticles. Notably, the elongation at break maintains relatively high values (>600%) even at higher ZnO loadings, indicating that the material retains its elastomeric character while gaining strength [22]. The modulus at 300% elongation (M300) increases progressively with ZnO content, from 2.3 MPa for unfilled XNBR to 5.8 MPa at 7.5 phr loading.

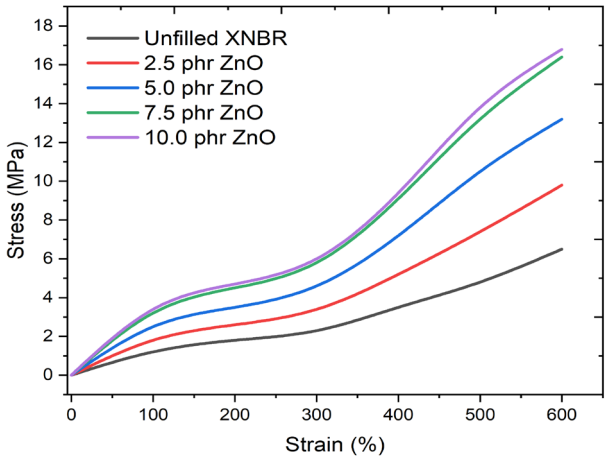

Fig. 3. Stress-strain curves of XNBR composites with varying ZnO content.

Dynamic mechanical analysis reveals significant changes in the viscoelastic behavior of the composites. The storage modulus (E') shows a substantial increase across the temperature range studied (-60°C to 100°C), particularly in the rubbery region (Figure 4). At room temperature (25°C),

the storage modulus increases from 3.2 MPa for unfilled XNBR to 7.8 MPa for the composite containing 7.5 phr ZnO.

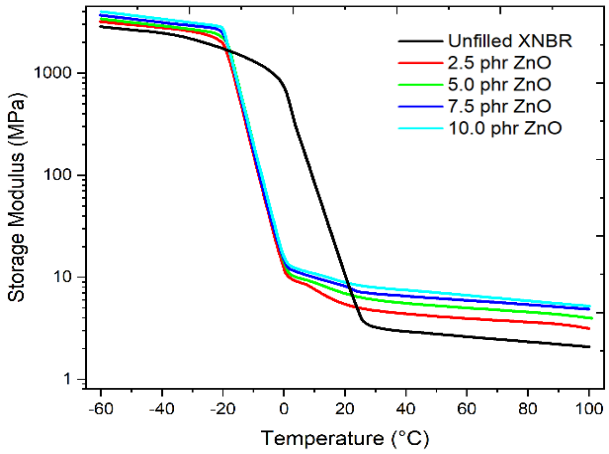

Fig. 4. Temperature dependence of storage modulus for XNBR/ZnO composites.

The tan δ curves (Figure 5) exhibit two distinct transitions: the primary α-transition corresponding to the glass transition temperature (Tg) and a secondary transition at higher temperatures attributed to the formation of ionic clusters [23]. The Tg shifts slightly towards higher temperatures with increasing ZnO content, suggesting restricted chain mobility due to strong polymer-filler interactions [24].

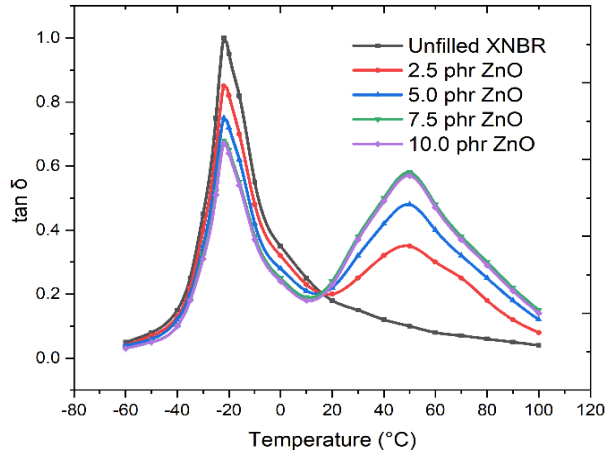

Fig. 5. Tan δ curves showing dual transition behavior in XNBR/ZnO composites.

The structure-property relationships indicate that the enhancement in mechanical properties can be attributed to several factors: (1) the efficient stress transfer enabled by the high aspect ratio of rod-like ZnO nanoparticles, (2) the formation of an interconnected network of ionic clusters acting as physical crosslinks, and (3) the strong interfacial interactions between the carboxyl groups of XNBR and the ZnO surface.

3.3. Tribological behavior

The incorporation of ZnO nanoparticles demonstrates significant improvements in the tribological properties of XNBR composites. The friction coefficient measurements, conducted under dry sliding conditions, reveal a systematic reduction with increasing ZnO content (Figure 6). The steady-state friction coefficient decreases from 0.82 for unfilled XNBR to 0.45 for the composite containing 7.5 phr ZnO, representing a 45% reduction. This improvement is attributed to the formation of a transfer film on the counterface, as evidenced by surface analysis [25].

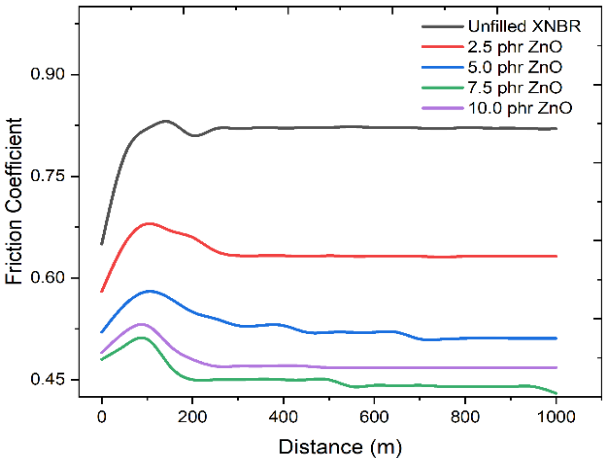

Fig. 6. Evolution of friction coefficient with sliding distance for XNBR/ZnO composites.

Wear resistance characteristics, quantified through specific wear rate measurements, show substantial enhancement with ZnO incorporation (Table 2). The specific wear rate decreases from 3.8×10^{-4} mm³/Nm for unfilled XNBR to 8.5×10^{-5} mm³/Nm at 7.5 phr ZnO loading, indicating a 78% improvement in wear resistance. Beyond 7.5 phr, marginal increases in wear rate are observed, possibly due to agglomeration effects [26].

Table 2. Tribological parameters of XNBR/ZnO composites at various loadings.

Parameter	**Unfilled XNBR**	**2.5 phr ZnO**	**5.0 phr ZnO**	**7.5 phr ZnO**	**10.0 phr ZnO**
Steady-state friction coefficient	0.82	0.65	0.52	0.45	0.47
Specific wear rate (10^{-4} mm³/Nm)	3.80	2.45	1.62	0.85	0.92
Surface roughness, Ra (μm)	2.85	2.24	1.86	1.45	1.52
Contact temperature rise (°C)	42.5	35.8	28.4	22.6	23.8
Transfer film thickness (μm)	-	2.8	3.5	4.2	4.0
Running-in period (m)	180	165	145	125	130

SEM analysis of worn surfaces (Figure 7) reveals distinct morphological differences between unfilled and ZnO-filled composites. The unfilled XNBR exhibits severe surface damage characterized by deep grooves and tear patterns, indicating adhesive wear mechanisms. In contrast, ZnO-filled composites show significantly smoother worn surfaces with minimal scoring marks, suggesting a transition to a milder abrasive wear regime. The mechanism of friction reduction can be attributed to three primary factors: (1) the formation of a stable transfer film facilitated by ZnO nanoparticles, which reduces direct contact between the composite and counterface [27]; (2) the enhanced mechanical strength of the composite surface, reducing deformation under sliding contact; and (3) the ability of rod-like ZnO particles to reorient parallel to the sliding direction, potentially providing a roller-bearing effect [28].

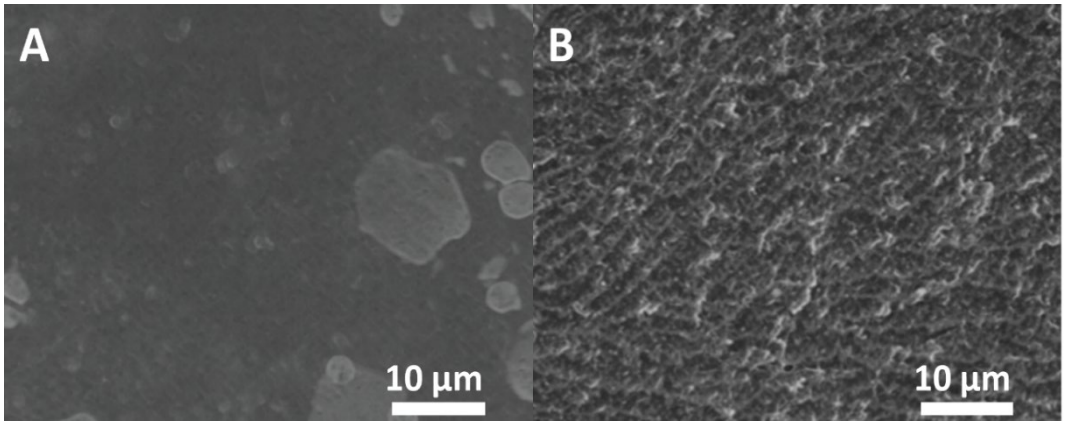

Fig. 7. SEM micrographs of worn surfaces: (A) unfilled XNBR, (B) XNBR/ZnO (7.5 phr).

3.4. Self-healing performance

The self-healing capabilities of XNBR/ZnO composites were evaluated through controlled damage-recovery experiments. Healing efficiency, defined as the ratio of recovered to original tensile strength, shows strong dependence on both temperature and healing time (Figure 8). At room temperature (25°C), modest healing efficiencies of 35-45% are achieved after 24 hours. However, healing efficiency increases dramatically at elevated temperatures, reaching 85% at 80°C for the 7.5 phr ZnO composite after 4 hours.

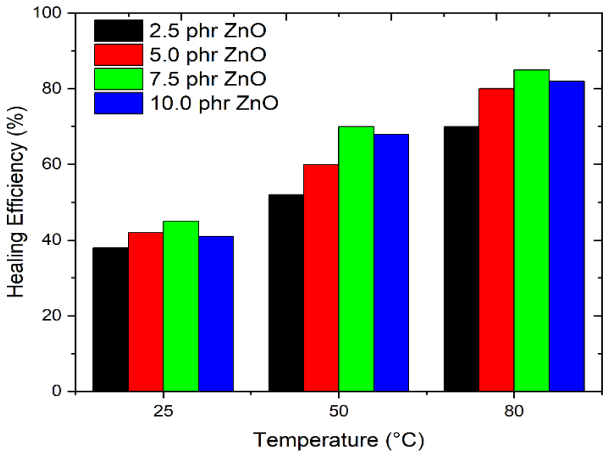

Fig. 8. Temperature-dependent healing efficiency of XNBR/ZnO composites.

Temperature dependence studies (Table 3) reveal an activation energy for healing of approximately 45 kJ/mol, suggesting that the process is governed by molecular diffusion and ionic bond reformation. The healing response shows significant enhancement above 60°C, corresponding to increased chain mobility and accelerated ionic cluster reorganization [29]. Time-dependent recovery analysis (Figure 9) demonstrates three distinct stages in the healing process: (1) an initial rapid recovery within the first 30 minutes, accounting for approximately 40% of the total healing; (2) a moderate recovery phase extending over 2-4 hours; and (3) a plateau region where additional healing becomes minimal. This behavior is consistent across all ZnO loadings, though the extent of recovery varies.

The self-healing mechanism in these composites operates through the dynamic nature of ionic crosslinks between ZnO nanoparticles and carboxyl groups in XNBR. Upon damage, the ionic bonds are temporarily disrupted. During the healing process, chain mobility enables the reformation of these ionic crosslinks across the damaged interface [30]. The rod-like morphology of ZnO particles appears to enhance this process by providing multiple contact points for ionic interaction, facilitating more efficient bridge formation across damaged surfaces.

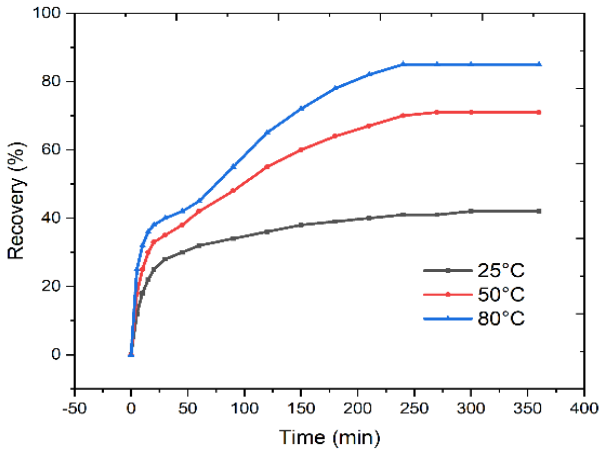

Fig. 9. Time-dependent recovery profiles at different temperatures for XNBR/ZnO (7.5 phr).

Table 3. Healing efficiency data at different temperatures and time intervals.

Temperature	Parameter	2.5 phr ZnO	5.0 phr ZnO	7.5 phr ZnO	10.0 phr ZnO
25°C	Initial recovery rate (%/min)	0.85	0.92	1.15	1.12
	Maximum healing efficiency (%)	38	42	45	44
	Time to 90% max healing (min)	840	780	720	735
50°C	Initial recovery rate (%/min)	1.25	1.45	1.85	1.80
	Maximum healing efficiency (%)	52	60	70	68
	Time to 90% max healing (min)	420	380	340	350
80°C	Initial recovery rate (%/min)	2.15	2.45	2.85	2.75
	Maximum healing efficiency (%)	70	80	85	82
	Time to 90% max healing (min)	180	165	150	155
Kinetic	Activation energy (kJ/mol)	42.5	43.8	45.2	44.8
Parameters	Pre-exponential factor (min^{-1})	4.2×10^4	4.8×10^4	5.5×10^4	5.3×10^4
	Correlation coefficient (R^2)	0.982	0.985	0.988	0.986

3.5. Thermal and dynamic properties

Dynamic mechanical analysis reveals significant modifications in the thermal and viscoelastic behavior of XNBR composites with ZnO incorporation. The glass transition temperature (Tg), determined from the peak of tan δ curves, exhibits a progressive shift from -22°C for unfilled XNBR to -16°C for composites containing 7.5 phr ZnO (Figure 10). This shift indicates restricted chain mobility due to the formation of ionic crosslinks between ZnO nanoparticles and carboxyl groups. Storage modulus (E') profiles demonstrate substantial reinforcement across the temperature range studied (-60°C to 100°C). At room temperature, E' increases from 3.2 MPa for unfilled XNBR to 8.5 MPa for 7.5 phr ZnO loading. Notably, the rubbery plateau region extends to higher temperatures with increasing ZnO content, indicating enhanced thermal stability of the network structure [31]. The loss modulus (E") curves show broadening of the transition peak, suggesting a wider distribution of relaxation times in the filled systems [32].

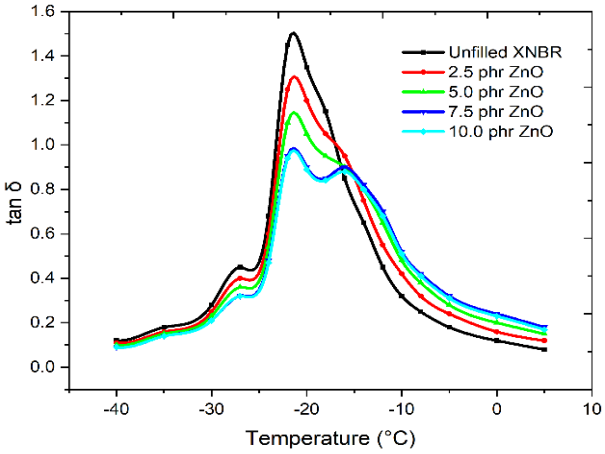

Fig. 10. Temperature dependence of tan δ for XNBR/ZnO composites showing Tg shifts.

Thermogravimetric analysis (Figure 11A) indicates improved thermal stability with ZnO incorporation. The onset temperature of degradation (T5%, temperature at 5% weight loss) increases from 385°C for unfilled XNBR to 412°C for the 7.5 phr ZnO composite. The char yield at 600°C also shows a corresponding increase from 8% to 15%, suggesting the formation of more thermally stable structures. The dynamic mechanical behavior exhibits strong frequency dependence, particularly in the transition region. Master curves constructed through time-temperature superposition (Figure 11B) reveal increased complex modulus values and reduced frequency dependence with ZnO loading, indicating the formation of a more robust network structure [33].

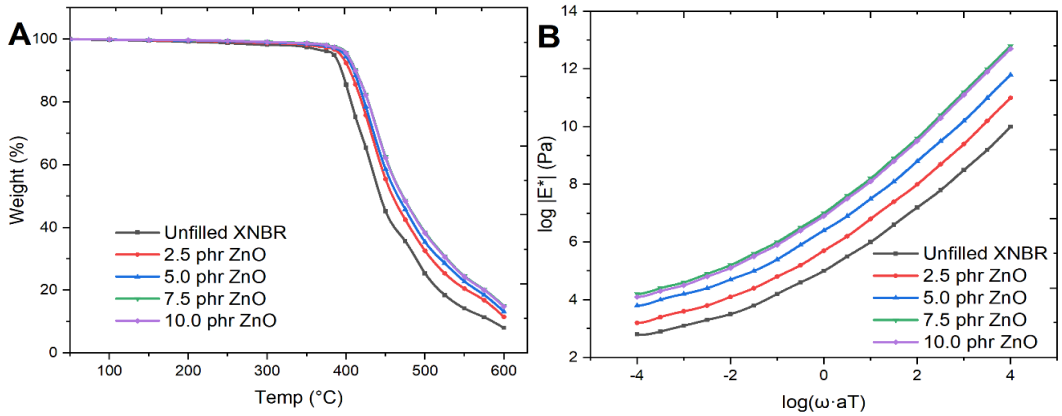

Fig. 11. (A) Thermogravimetric analysis curves showing enhanced thermal stability with ZnO loading. (B) Master curves of complex modulus for XNBR/ZnO composites at different loadings (Tref = 25°C).

3.6. Structure-property correlations

The influence of ZnO content on composite properties follows a non-linear trend, with optimal performance typically observed at 7.5 phr loading. The initial rapid improvement in properties up to 5 phr can be attributed to the formation of an effective ionic network. Beyond 7.5

phr, property deterioration occurs due to particle agglomeration and network saturation effects. Particle size analysis reveals critical relationships between ZnO dimensions and composite performance. The rod-like morphology (aspect ratio ~11:1) proves particularly effective in forming a percolated network structure at lower loadings compared to spherical particles. The nanoscale dimensions ensure high surface area for ionic interactions while maintaining good dispersion characteristics up to the optimal loading level [34].

Processing-structure relationships demonstrate strong dependence on mixing conditions and thermal history. Extended mixing times (>20 minutes) lead to reduced aspect ratios of ZnO particles through mechanical breakdown, compromising reinforcement efficiency. The processing temperature window of 140-160 ° C proves optimal for achieving uniform dispersion while preserving particle morphology. The structure-property-performance relationships can be understood through a hierarchical model of reinforcement mechanisms. Primary reinforcement occurs through ionic crosslinking between ZnO surfaces and carboxyl groups, creating physical crosslinks. Secondary reinforcement derives from the formation of a percolated network of ZnO particles, providing additional mechanical support [35]. The combination of these mechanisms results in synergistic enhancement of mechanical, thermal, and self-healing properties.

The efficiency of property enhancement correlates strongly with the degree of ionic cluster formation, as evidenced by FTIR analysis showing progressive reduction in free carboxyl groups with increasing ZnO content. The optimal balance between ionic crosslinking and matrix mobility occurs at 7.5 phr loading, explaining the peak in performance properties at this concentration.

4. Conclusion

In this comprehensive study, the incorporation of rod-like ZnO nanoparticles (average length 450±50 nm, diameter 40±10 nm) into XNBR demonstrated significant enhancements in mechanical, tribological, and self-healing properties. The optimal ZnO loading of 7.5 phr resulted in a 125% increase in tensile strength (reaching 18.5 MPa) and a 45% reduction in friction coefficient (decreasing from 0.82 to 0.45) compared to unfilled XNBR. The specific wear rate showed remarkable improvement, reducing by 78% from 3.8×10^{-4} to 8.5×10^{-5} mm^3/Nm. Self-healing capabilities exhibited strong temperature dependence, achieving up to 85% healing efficiency at 80°C within 4 hours, with an activation energy of approximately 45 kJ/mol. The glass transition temperature shifted from -22°C to -16°C, indicating enhanced polymer-filler interactions, while thermal stability improved with the onset degradation temperature increasing from 385°C to 412°C.

The rod-like morphology of ZnO nanoparticles proved particularly effective in forming a percolated network structure, facilitating both mechanical reinforcement and ionic crosslinking. The synergistic effects of ionic cluster formation and mechanical reinforcement resulted in optimal performance at 7.5 phr loading, beyond which property deterioration occurred due to agglomeration effects. These findings provide valuable insights for developing high-performance rubber composites with enhanced durability and self-healing capabilities for demanding industrial applications.

Acknowledgements

This work was supported by Key Research and Development Program of Gansu Province (No. 23YFGA0020).

References

[1] N. A. S. Abdullah, F. F. Abdullah, A. H. Sufian, A. N. S. Z. Abidin, A. S. Jamaludin, M. N. M. Razali, Innovative Manufacturing, Mechatronics & Materials Forum 2021 48, 1941 (2022); https://doi.org/10.1016/j.matpr.2021.10.247

[2] I. Veza, Z. Zainuddin, N. Tamaldin, M. Idris, I. Irianto, I. M. R. Fattah, Results in Engineering 16, 100787 (2022); https://doi.org/10.1016/j.rineng.2022.100787

[3] A. Nihmath, M. T. Ramesan, Polymer Testing 89, 106728 (2020); https://doi.org/10.1016/j.polymertesting.2020.106728

[4] M. F. Bidgoli, F. Arabgol, M. Kokabi, Iranian Polymer Journal 29, 985 (2020); https://doi.org/10.1007/s13726-020-00855-z

[5] C. Porter, B. Zaman, R. Pazur, Polymer Degradation and Stability 206, 110199 (2022); https://doi.org/10.1016/j.polymdegradstab.2022.110199

[6] G. L. Rempel, H. Wang, in Rubber Nano Blends: Preparation, Characterization and Applications, G. Markovic and V. P. M., eds. (Springer International Publishing, 2017), pp. 67-88; https://doi.org/10.1007/978-3-319-48720-5_3

[7] M. Zemzem, L. Vinches, S. Hallé, Journal of Applied Polymer Science 134, 45350 (2017); https://doi.org/10.1002/app.45350

[8] S. Sahoo, A. K. Bhowmick, Journal of Applied Polymer Science 106, 3077 (2007); https://doi.org/10.1002/app.24832

[9] W. Yang, C. Wang, Z. Liu, J. Tan, Polymer Composites 43, 4588 (2022); https://doi.org/10.1002/pc.26714

[10] M. K. Hafshejani, M. Afrasiabi, M. Khazaei, A. Langari, Life Science Journal 10, 3597 (2013).

[11] S. Utrera-Barrios, J. Araujo-Morera, L. Pulido de Los Reyes, R. Verdugo Manzanares, R. Verdejo, M. Á. López-Manchado, M. Hernández Santana, European Polymer Journal 139, 110032 (2020); https://doi.org/10.1016/j.eurpolymj.2020.110032

[12] Z. F. Zhang, X. T. Liu, K. Yang, S. G. Zhao, Macromolecular Research 27, 803 (2019); https://doi.org/10.1007/s13233-019-7110-8

[13] M. Das, T. K. Sreethu, S. Pal, K. Naskar, ACS Applied Polymer Materials 4, 6414 (2022); https://doi.org/10.1021/acsapm.2c00840

[14] D. Y. S. Low, J. Supramaniam, B. H. Goh, S. Manickam, S. Y. Tang, Advanced Functional Materials 34, 2401345 (2024).

[15] S. W. Wajge, D. Basu, A. Das, S. Mandal, P. K. Maji, S. Singh, C. Das, Journal of Polymer Science 62, 2103 (2024); https://doi.org/10.1002/pol.20230800

[16] K. Roy, S. C. Debnath, A. Pongwisuthiruchte, P. Potiyaraj, ACS Omega 6, 9975 (2021);

https://doi.org/10.1021/acsomega.0c05743

[17] L. Feng, H. Zhao, X. He, Y. Zhao, L. Gou, Y. Wang, Polymer Engineering & Science 59, 1603 (2019); https://doi.org/10.1002/pen.25158

[18] P. K. Behera, S. Mohanty, V. K. Gupta, Polymer Chemistry 12, 1598 (2021); https://doi.org/10.1039/D0PY01458C

[19] M. Vafaee, M. S. Ghamsari, Materials Letters 61, 3265 (2007); https://doi.org/10.1016/j.matlet.2006.11.089

[20] C. Wu, X. Qiao, J. Chen, H. Wang, F. Tan, S. Li, Materials Letters 60, 1828 (2006); https://doi.org/10.1016/j.matlet.2005.12.046

[21] D. Raoufi, Renewable Energy 50, 932 (2013); https://doi.org/10.1016/j.renene.2012.08.076

[22] D. Ponnamma, K. K. Sadasivuni, Y. Grohens, Q. Guo, S. Thomas, Journal of Materials Chemistry C 2, 8446 (2014); https://doi.org/10.1039/C4TC01037J

[23] E. Pregi, D. Kun, A. Wacha, B. Pukánszky, European Polymer Journal 142, 110110 (2021); https://doi.org/10.1016/j.eurpolymj.2020.110110

[24] A. De Barros, L. Farenzena, D. Andrade, E. Da Silveira, K. Wien, The Journal of Physical Chemistry C 115, 12005 (2011); https://doi.org/10.1021/jp111152y

[25] H. Li, Z. Yin, D. Jiang, L. Jin, Y. Cui, Wear 328-329, 17 (2015); https://doi.org/10.1016/j.wear.2015.01.028

[26] H. Qi, G. Li, G. Zhang, T. Wang, Q. Wang, Materials & Design 109, 367 (2016); https://doi.org/10.1016/j.matdes.2016.07.088

[27] J. Ye, D. L. Burris, T. Xie, Lubricants 4, 4 (2016); https://doi.org/10.3390/lubricants4010004

[28] M. H. Cho, Journal of Mechanical Science and Technology 23, 2291 (2009); https://doi.org/10.1007/s12206-009-0354-z

[29] J. Ye, H. S. Khare, D. L. Burris, Wear 297, 1095 (2013); https://doi.org/10.1016/j.wear.2012.12.002

[30] S. Utrera-Barrios, R. Verdejo, M. A. López-Manchado, M. H. Santana, Materials Horizons 7, 2882 (2020); https://doi.org/10.1039/D0MH00535E

[31] N. F. Mohd Sani, H. J. Yee, N. Othman, A. A. Talib, R. K. Shuib, Polymer Testing 111, 107598 (2022); https://doi.org/10.1016/j.polymertesting.2022.107598

[32] S. Utrera-Barrios, M. Hernández Santana, R. Verdejo, M. A. López-Manchado, ACS Omega 5, 1902 (2020); https://doi.org/10.1021/acsomega.9b03516

[33] N. Hohlbein, A. Shaaban, A. R. Bras, W. Pyckhout-Hintzen, A. M. Schmidt, Physical Chemistry Chemical Physics 17, 21005 (2015); https://doi.org/10.1039/C5CP00620A

[34] J. Boden, C. R. Bowen, A. Buchard, M. G. Davidson, C. Norris, ACS Omega 7, 15098 (2022); https://doi.org/10.1021/acsomega.2c00971

[35] D. Wang, J. Guo, H. Zhang, B. Cheng, H. Shen, N. Zhao, J. Xu, Journal of Materials Chemistry A 3, 12864 (2015); https://doi.org/10.1039/C5TA01915J